

Buckling-regulated bandgaps of soft metamaterials with chiral hierarchical microstructure

Hui-Kai Zhang, Xi-Qiao Feng*

Department of Engineering Mechanics & State Key Laboratory of Tribology, Tsinghua University, Beijing 100084, China



ARTICLE INFO

Article history:

Received 3 December 2020

Received in revised form 30 December 2020

Accepted 31 December 2020

Available online 5 January 2021

Keywords:

Soft metamaterials

Hierarchical structure

Chirality

Postbuckling

Elastic wave bandgap

ABSTRACT

In traditional phononic metamaterials, elastic wave bandgaps are usually tuned by introducing periodic rigid inclusions in a soft matrix, but they are difficult to adapt to the changes of external mechanical environments. In this paper, inspired by the strategies of biological materials to achieve specific functions, we propose a kind of soft metamaterials with chiral and hierarchical structures. Their elastic wave bandgaps can be easily regulated in a larger space of frequency by means of the postbuckling-induced evolution of microstructures under loading. The postbuckling behavior of chiral hierarchical structures is investigated through finite element simulations and compared with those of symmetric hierarchical structures. The stress-strain curves, the phase diagram of uniaxial critical compressive strength, and the tunable elastic wave bandgaps of the proposed metamaterials are analyzed.

© 2021 Elsevier Ltd. All rights reserved.

1. Introduction

In classical phononic crystal materials, periodically distributed rigid inclusions of specific shapes are often introduced into a softer matrix, and thereby the local resonance mechanism is utilized to inhibit the propagation of elastic waves in a certain range of frequency [1,2]. However, the elastic wave bandgaps of this kind of metamaterials are difficult to adapt to the changes of the external mechanical environments. In recent years, therefore, soft metamaterials with easily tunable elastic wave bandgaps have attracted much attention due to their technologically significant applications.

In nature, many organisms (e.g., octopus tentacles and snakes) combine their rigid skeleton structures and soft components to achieve a diversity of biological functions. Soft materials can undergo large deformation under such external stimuli as mechanical, thermal, and electrical fields. Soft functional materials have found ever increasing applications in the fields of, for examples, metamaterials [3–5], flexible devices and robotics [6–10], mechanical characterization [11], biomimetic 4D printing [12], artificial tissues, and biomedical engineering [13–15].

Almost all biological materials possess hierarchical structures ranging from nano, micro to macro scales, which are crucial to achieve their mechanical properties and biological functions. For example, hierarchical structures endow the wings of butterflies with rich colors, self-cleaning ability, and directional fluorescence emission [16–18]. Owing to its hierarchical structures, the glass

sponge skeleton exhibits an outstanding combination of high mechanical stiffness, strength, toughness, stability, and elasticity [19,20]. Hierarchical cell-laden GelMA hydrogel obtained from 3D extrusion bioprinting [21] shows a high recoverability of deformation and the functions of highly maintaining cell vitality, proliferation, diffusion and differentiation. Moreover, inspired by biological materials, structural hierarchy has been proposed as a strategy to achieve superior mechanical properties and various functions of materials [4,22].

In addition, chirality is an intrinsic geometric feature of the hierarchical structures in biological materials, such as right- and left-handed sea shells, DNA double helixes, plant climbing tendrils [23]. Due to the effects of geometric asymmetry, chiral structures can render some unusual behaviors, such as tension–torsion coupling deformations [24,25], negative thermal expansion [23], and gyration of impacting droplets [26].

For most traditional engineering structures made of such hard materials as steel and concrete, buckling is a typical mechanism that often causes structural failure and thus should be avoided. In contrast, global and/or local buckling is a key mechanism that drives the morphogenesis of biological tissues and organs, such as the convolutional development of brains [27], the self-organization of epidermal tissues [28], the surface wrinkling of airway and esophagus [6], and the morphological evolution of seed pods during dehydration [6]. Buckling has also been utilized in the design of pneumatic-driven robotics [7,8,29] and mechanical metamaterials with negative swelling [30], negative Poisson's ratio [3], and abnormal deformation behavior [31].

Recent researches demonstrated that the elastic wave bandgaps of soft materials with periodically distributed holes

* Corresponding author.

E-mail address: fengxq@tsinghua.edu.cn (X.-Q. Feng).

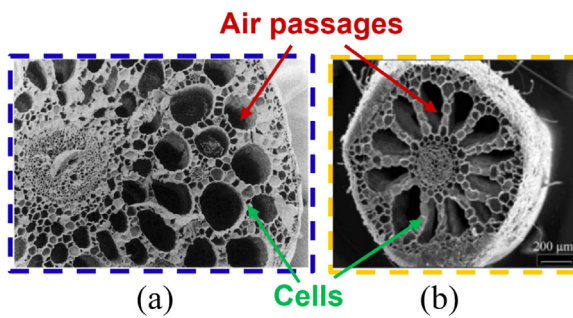


Fig. 1. (a) Hierarchical structure of a stem tissue of aquatic plant, *potamogeton pectinatus* [32]. (b) Wheel-shaped aerenchyma (WA), *myriophyllum spicatum* [33]. Source: Reprinted from Ref. [32] and [33] with permission.

can be tuned easily through the topological evolution during the process of postbuckling [34–37]. Moreover, soft optical metamaterials have been designed that can transform from a two-dimensional structure to a three-dimensional one by triggering out-of-plane deformation modes through soft pneumatic or mechanical load, and the deformed structures may exhibit greatly different properties of energy transmission and polarization azimuth-angle rotation from the original, undeformed structure [38,39]. In contrast to the classical phononic crystal, utilizing the buckling of soft periodic microstructures seems a strategy to improve the flexibility of metamaterials to tune phononic functionality in a larger space. However, it remains an unsolved issue how soft hierarchical structures can be designed to tune the phononic bandgaps of metamaterials in a wide range of frequency.

In this paper, inspired by the hierarchical tissues of aquatic plants [Fig. 1(a) and (b)] [32,33], we propose a strategy to design a kind of soft phononic metamaterials, consisting of hierarchical microstructures. In Section 2 of this letter, we construct the Computer Aided Design (CAD) models of materials with hierarchical, either chiral or symmetric, microstructures. In Section 3, the deformation and postbuckling behaviors of the proposed materials are analyzed with respect to the variations in hierarchical structural parameters through finite element simulations. In Section 4, we explore how to regulate the functionality of the elastic wave bandgaps through soft hierarchical structures.

2. Design of hierarchical structures

In this work, inspired by the polygonal hierarchical aerenchyma in aquatic plants shown in Fig. 1(a) and (b), we propose a class of metamaterials with two-dimensional hierarchical and chiral structures, as shown in Fig. 2(a) and (b). The chiral hierarchical structure [Fig. 2(c) and (d)] is obtained from the topology optimization method with the objective of maximized stiffness under a given porosity and multi-load condition [40]. To investigate the significant effect of chirality, we compare the chiral hierarchical structures with those with similar but symmetric truss microstructure shown in Fig. 3(a) and (b). The symmetric truss microstructure shown in Fig. 3(c) and (d) is derived from the chiral structure in Fig. 2(d).

In reality, this kind of hierarchical structures can be produced by using the 3D printing technique or by assembling small-sized, either chiral or symmetric, building elements. Such soft materials as PDMS and silicone rubber can be used for this purpose. In this paper, the constituent material is assumed to obey the incompressible hyperelastic neo-Hookean constitutive model. Its elastic strain energy density function can be written as

$$U = C_{10} (\bar{I}_1 - 3) + \frac{1}{D_1} (J^{el} - 1)^2, \quad (1)$$

where C_{10} and D_1 are the material parameters, and \bar{I}_1 and J^{el} are the first deviatoric invariant and the elastic volume ratio, respectively.

3. Postbuckling analysis of hierarchical structures

3.1. Simulation method of buckling

In the examples, we take the length l_1 and material volume fraction of all first-order microstructures as 60 mm and 0.5, respectively. The rotation angle of the chiral microstructure and the wall thickness of symmetric microstructure are set as $\theta = 11.6^\circ$ and $t = 5.64$ mm. We take the parameters $c = 8.5$ mm and $d = 11.7$ mm. Each second-order hierarchical beam comprises 12 microstructures assembled in a series manner.

The pseudodynamic method [41] is adopted to simulate the global postbuckling of the soft hierarchical structures and the local buckling of their constituent struts. We firstly conduct the

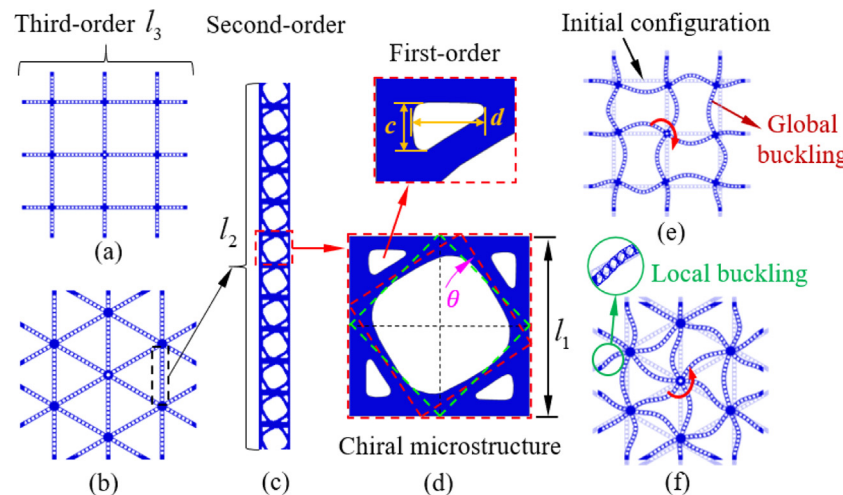


Fig. 2. Two chiral hierarchical structures and their chiral postbuckling. (a) Third-order chiral quadrilateral hierarchical structure with length l_3 . (b) Third-order chiral triangular hierarchical structure. (c) Second-order chiral hierarchical beam with length l_2 . (d) First-order chiral microstructure with length l_1 and rotation angle θ . c and d are the length of the internal triangle voids. (e) Twisting deformation of quadrilateral chiral hierarchical structure. (f) Twisting deformation of triangular hierarchical structure. (For interpretation of the references to color in this figure legend, the reader is referred to the web version of this article.)

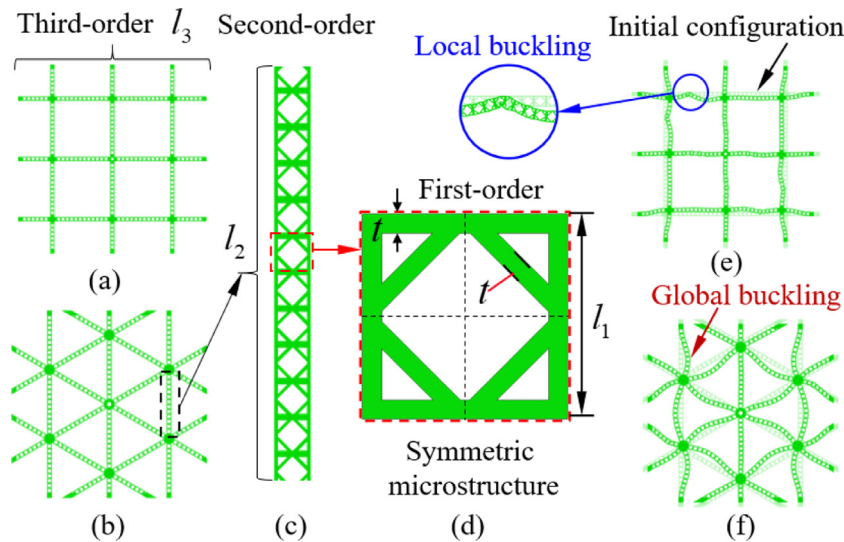


Fig. 3. Two symmetric soft hierarchical structures and their symmetric postbuckling. (a) Third-order symmetric quadrilateral hierarchical structure with length l_3 . (b) Third-order symmetric triangular hierarchical structure. (c) Second-order symmetric hierarchical beam with length l_2 . (d) First-order symmetric microstructure with length l_1 and uniform wall thickness t . (e) Symmetric deformation of quadrilateral hierarchical structure. (f) Symmetric deformation of triangular hierarchical structure.

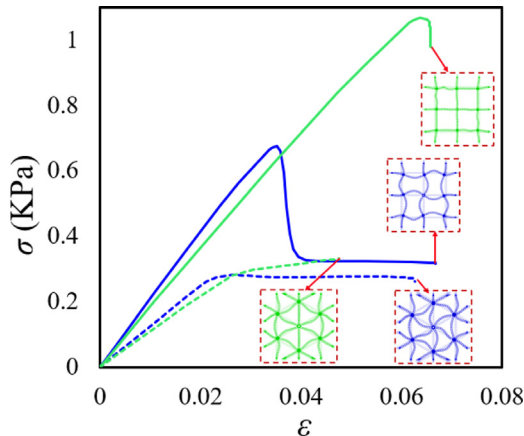


Fig. 4. Stress-strain curves of soft hierarchical structures under biaxial compression.

linear buckling analysis by using the subspace method of the soft hierarchical structures shown in Figs. 2 and 3 under biaxial compression. Then, the 0.0001 time of the first buckling mode is introduced as the initial defects for the postbuckling analysis under biaxial compression.

For silicone rubber, the coefficients are set to be $C_{10} = 0.00978$ and $D = 1.0025$ in the commercial software Abaqus [42]. The material density is $\rho = 1050 \text{ kg/m}^3$. To avoid the interpenetration of internal structures during deformation, we apply general contact to all structures with a coefficient of friction being 0.1. In our simulations, all soft hierarchical structures are discretized into CPS3H elements.

3.2. Postbuckling of hierarchical structures

The evolutions of the soft hierarchical structures during postbuckling are shown in Figs. 2(e, f) and 3(e, f). It is seen that the second-order hierarchical beams consisting of chiral microstructures rotate along the central joints [the red arrows in Fig. 2(e) and (f)]. However, the second-order hierarchical beams comprising symmetric microstructures have approximately symmetric

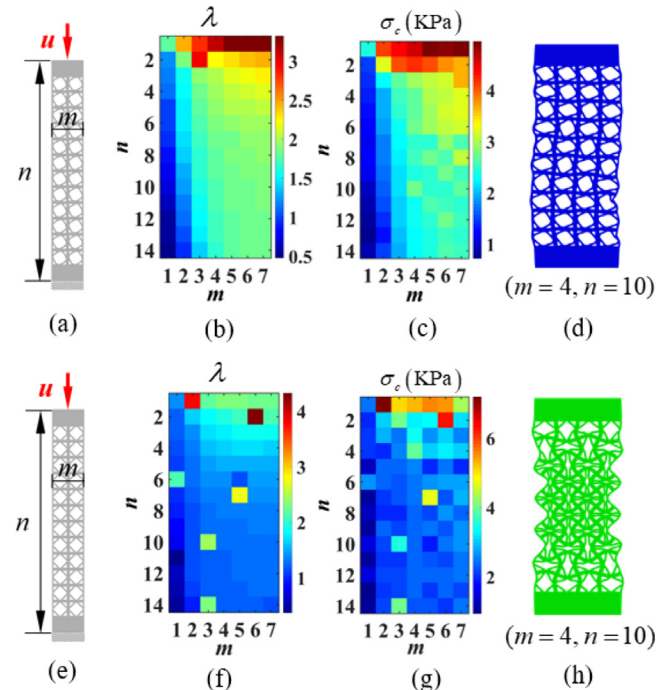


Fig. 5. Buckling modes and critical compressive strengths of chiral second-order hierarchical beams with different numbers m and n in the x and y directions. (a) Calculation model of a chiral hierarchical beam. (b) Phase diagram for the eigenvalues of chiral hierarchical beams with different (m, n) . (c) Phase diagram for the critical buckling stresses of chiral hierarchical beams with different (m, n) . (d) Deformation modes of a chiral hierarchical beam with $(m, n) = (4, 10)$. (e) Calculation model of symmetric hierarchical beams. (f) Phase diagram for the linear eigenvalues of symmetric hierarchical beams. (g) Phase diagram for the critical compressive strength of symmetric hierarchical beams. (h) Deformation modes of a symmetric hierarchical beam with $(m, n) = (4, 10)$. The bright voxel points in Fig. 5(f) and (g) are caused by the repeated eigenvalues of the symmetric structure in the linear buckling analysis.

deformation forms during postbuckling, as shown in Fig. 3(c) and (d).

Our simulations show that the hierarchical chiral microstructures are easier to buckle, and the hierarchical beams rotate along

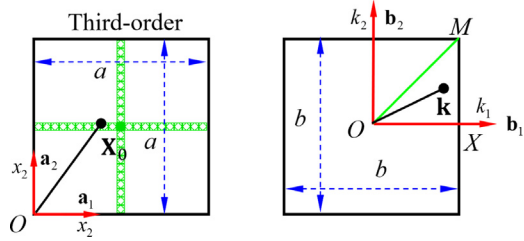


Fig. 6. (a) Schematic diagram of a square third-order hierarchical unit cell with length a . (b) The square reciprocal unit cell with length b .

the central joints during postbuckling under biaxial compression. Due to this global rotation mode of beams, the hierarchical structures buckle in a chiral manner, leading to a lower value of critical buckling strain, as shown by the stress-strain curves in Fig. 4. The chiral hierarchical structures (both quadrilateral and triangular structures) have a smaller critical compressive strength and a lower critical buckling strain than the symmetric hierarchical structures. By virtue of this chiral buckling mechanism, the elastic wave bandgaps of chiral hierarchical structures can be tuned more efficiently, as we will demonstrate below.

3.3. Chiral postbuckling of hierarchical beams

As shown in the zoomed graphs of Figs. 2(f) and 3(e), the deformations of the hierarchical structures involve multiple bifurcations during the process of postbuckling [43–45]. The buckling of microstructure also affects the load-bearing capacity of the hierarchical structures. In Fig. 5(a) and (e), we construct a series of second-order hierarchical beams through tuning the parameters

$m \in [1, 7]^{N^+}$ in the x horizontal direction and $n \in [1, 14]^{N^+}$ in the y direction. The corresponding results of simulations are given in Fig. 5(a) and (e).

It is seen that the eigenvalues λ [Fig. 5(b)] and the critical strengths σ_c [Fig. 5(c)] are smaller than those in Fig. 5(f) and (g) for all combinations of (m, n) . This means that the chiral structures deform easily and have a lower load-bearing capacity than the symmetric structures. This is attributed to the global rotational deformation mode during the buckling process of the structures consisting of chiral elements [Fig. 5(d)]. In comparison, for the structures consisting of symmetric microstructures, multiple local buckling patterns may occur [Fig. 5(h)]. Due to the chiral buckling mechanism of rotation, the chiral hierarchical structures show a lower load-bearing capacity than the symmetric structures. This phenomenon helps understand the findings given in Fig. 4. It is noted that Fig. 5(f) and (g) have some bright voxel points, which are caused by the repeated eigenvalues of the symmetric structure in the linear buckling analysis.

4. Bandgap analysis

4.1. Method

Soft single-level structures have been proposed to tune the elastic wave bandgaps through large deformation [34,35]. However, hierarchical structures have distinct advantages to achieve multiple functions of metamaterials, just like the rich color and superhydrophobicity of moth and dragonfly wings [29,46]. In this section, we explore the regulation of elastic wave bandgaps in soft hierarchical structures consisting of chiral [Fig. 2(d)] and symmetric [Fig. 3(d)] microstructures.

The analysis method of elastic wave bandgaps contains the following three steps. First, the postbuckling of the hierarchical

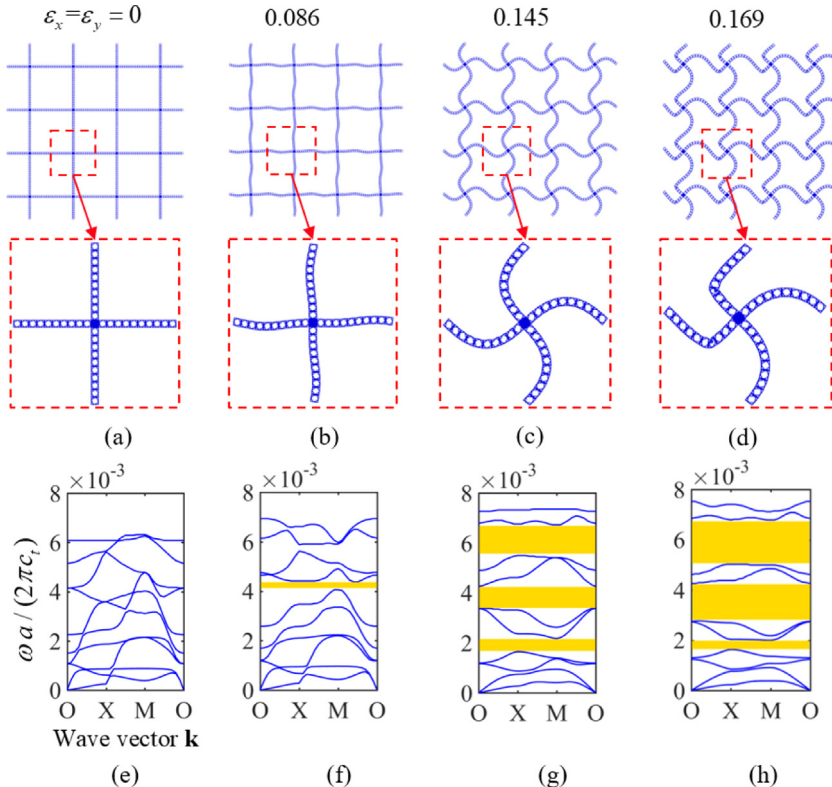


Fig. 7. Elastic wave bandgaps of soft, chiral and hierarchical structures. (a) Initial configuration with $\varepsilon_x = \varepsilon_y = 0$. (b) Postbuckling under strain $\varepsilon_x = \varepsilon_y = 0.086$. (c) Postbuckling under strain $\varepsilon_x = \varepsilon_y = 0.145$. (d) Postbuckling under strain $\varepsilon_x = \varepsilon_y = 0.169$. (e) Dispersive curves of the structure in Fig. 7(a). (f) Dispersive curves and bandgap of the structure in Fig. 7(b). (g) Dispersive curves and bandgaps of the structure in Fig. 7(c). (h) Dispersive curves and bandgaps of the structure in Fig. 7(d).

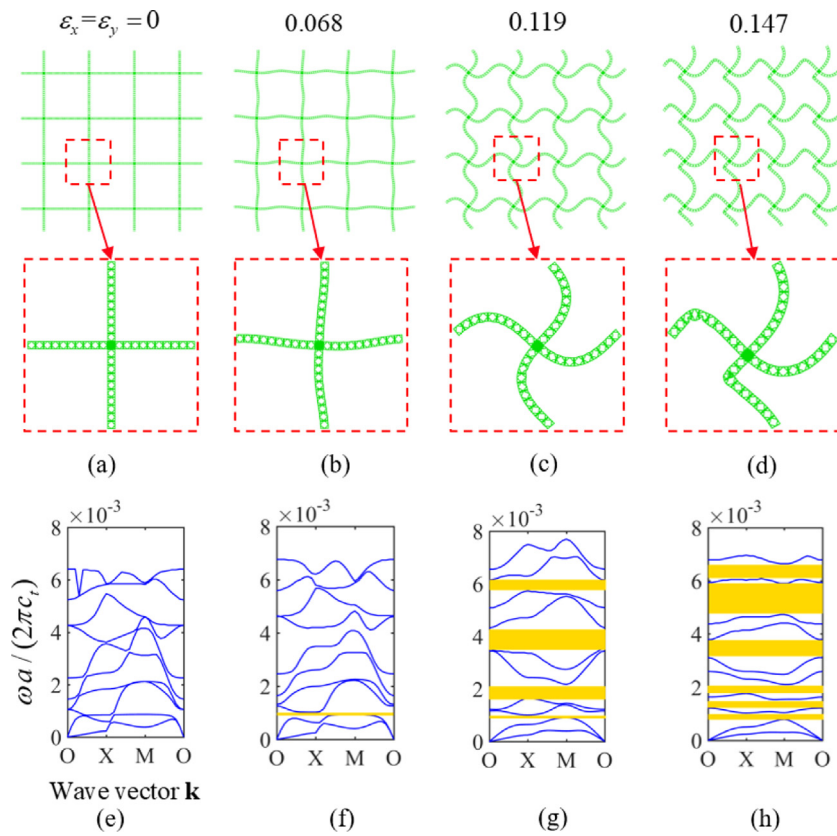


Fig. 8. Bandgaps of soft, symmetric and hierarchical structures. (a) Initial configuration with $\varepsilon_x = \varepsilon_y = 0$. (b) Postbuckling under strain $\varepsilon_x = \varepsilon_y = 0.0678$. (c) Postbuckling under strain $\varepsilon_x = \varepsilon_y = 0.119$. (d) Postbuckling under strain $\varepsilon_x = \varepsilon_y = 0.149$. (e) Dispersive curves of the structure in Fig. 8(a). (f) Dispersive curves and bandgap of the structure in Fig. 8(b). (g) Dispersive curves and bandgaps of the structure in Fig. 8(c). (h) Dispersive curves and bandgaps of the structure in Fig. 8(d).

structures is simulated by using Abaqus under displacement-controlled loading. In the simulations, periodic boundary conditions are applied on the third-order hierarchical unit cell by modifying the *Equation* module in Abaqus as

$$\mathbf{u}^+ - \mathbf{u}^- = \boldsymbol{\varepsilon}^* \mathbf{a}, \quad (2)$$

where the vector \mathbf{u} is the boundary nodal displacement vector, $\boldsymbol{\varepsilon}^*$ is the applied strain, and a is the length of the third-order hierarchical unit cell [Fig. 6(a)]. The superscripts '+' and '-' indicate the parameters on the two opposite edges.

Second, we export the deformed configuration to the elastic wave bandgap analysis. Bloch periodic boundary conditions are applied to this structure without considering its stress distribution induced by buckling [35]. The Bloch periodic boundary conditions can be written as [34–36]

$$\mathbf{u}(\mathbf{x}_0 + \mathbf{r}) = \mathbf{u}(\mathbf{x}_0) e^{i\mathbf{k}\cdot\mathbf{a}}, \quad (3)$$

where the vector \mathbf{u} is the displacement field, $\mathbf{x}_0 = (x_1, x_2)$ is the coordinate vector of the unit cell [Fig. 6(a)], and $\mathbf{r} = a \mathbf{n}_i$ ($i = 1, 2$), with \mathbf{n}_i being the unit directional vector. $\mathbf{k} = (k_1, k_2)$ is the wave vector in the reciprocal unit cell [Fig. 6(b)], and $k_1, k_2 \in [-\pi/a, \pi/a]$. For the square hierarchical unit cell in Fig. 6(a), the periodic vectors are $\mathbf{a}_1 = a(1, 0)$ and $\mathbf{a}_2 = a(0, 1)$, while its square reciprocal unit cell in Fig. 6(b) has $\mathbf{b}_1 = b(1, 0)$ and $\mathbf{b}_2 = b(0, 1)$. They satisfy the relation $\mathbf{a}_i \mathbf{b}_j = 2\pi \delta_{ij}$ ($i, j = 1, 2$), where δ_{ij} is the Kronecker delta.

In the third step, due to the symmetry of the square unit cell, we use the eigenfrequency analysis module in Abaqus to compute the dispersive curves with the wavevector \mathbf{k} sweeping along the first irreducible Brillouin zone $O - X - M - O$ [Fig. 6(b)].

4.2. Bandgap analysis

In order to illustrate the prominent features of chiral hierarchical structures in the regulation of elastic wave bandgaps, we compare the elastic wave propagation behaviors of the chiral and symmetric structures in Figs. 2(a) and 3(a). In the simulations, each second-order hierarchical beam has 10 microstructural elements. The numerical results are shown in Figs. 7 and 8, respectively. The normalized dispersive curves of $\omega a / (2\pi c_t)$ in Figs. 7(e) and 8(e) do not have any elastic wave bandgaps at the initial periodic configuration of the soft hierarchical structures, where $c_t = \sqrt{\mu_0/\rho}$ and μ_0 are the elastic shear wave speed and the initial shear modulus, respectively. As the applied strain increases, a few bandgaps appear gradually in the dispersive curves of the deformed structures. The first bandgap [Fig. 7(f)] occurs in the high frequency region under strain $\varepsilon_x = \varepsilon_y = 0.086$. With further loading, three bandgaps [Fig. 7(g)] appear in the low and high frequency regions under strain $\varepsilon_x = \varepsilon_y = 0.145$. Importantly, it is found that the number of bandgaps does not change as the applied strain increases from $\varepsilon_x = \varepsilon_y = 0.145$ [Fig. 7(g)] to $\varepsilon_x = \varepsilon_y = 0.169$ [Fig. 7(h)]. This robustness of elastic wave bandgaps is of significance for engineering application.

For the hierarchical structure with symmetric microstructural elements [Fig. 8(a)], the first bandgap [Fig. 8(f)] occurs in the low frequency region under strain $\varepsilon_x = \varepsilon_y = 0.068$. Four bandgaps appear in the low and high frequency regions [Fig. 8(g)] when the strain increases to $\varepsilon_x = \varepsilon_y = 0.119$. However, in contrast to the high robustness of the chiral structures, the number of bandgaps in the symmetric structure is greatly affected by the local buckling of the first-order structures [Fig. 8(d)]. This is because for the chiral hierarchical structures, the chiral building

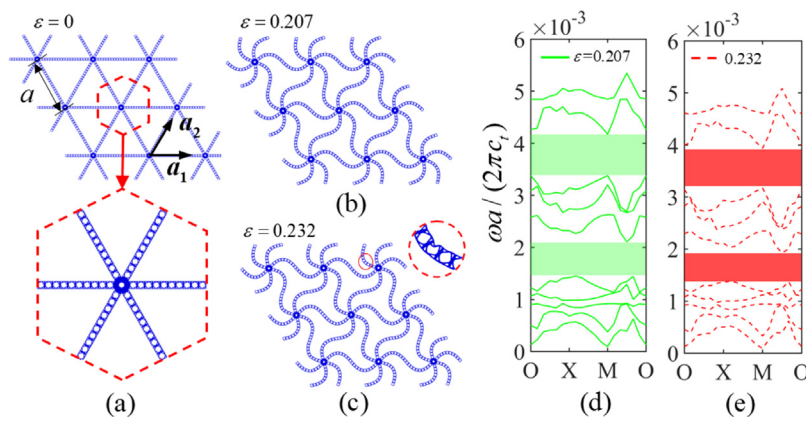


Fig. 9. Postbuckling and bandgaps of soft, triangular and hierarchical structures consisting of chiral unit cells. (a) Initial configuration with $\varepsilon = 0$. (b) Postbuckling under strain $\varepsilon = 0.207$. (c) Postbuckling under strain $\varepsilon = 0.232$. (d) Dispersive curves and bandgaps under strain $\varepsilon = 0.207$. (e) Dispersive curves and bandgaps under strain $\varepsilon = 0.232$.

elements bring the system into the global chiral buckling mode, while the symmetric structure may evolve into some other modes during postbuckling.

To further confirm this finding, we also analyze the postbuckling and elastic wave bandgaps of triangular hierarchical structures consisting of chiral unit cells, as shown in Fig. 9. As the applied strain increases from $\varepsilon = 0.207$ [Fig. 9(b)] to $\varepsilon = 0.232$ [Fig. 9(c)], local buckling occurs in the second-order structures [Fig. 9(c)]. During postbuckling, the number of elastic wave bandgaps [Fig. 9(d) and (e)] also keeps constant, in consistency with the conclusion drawn from Figs. 7 and 8. Therefore, the chiral hierarchical structures should have better performance for the application as phononic metamaterials.

5. Conclusions

Inspired by the strategy of biological materials to achieve multiple functions, we have proposed a class of soft metamaterials with chiral and hierarchical structures, which are demonstrated to have better performance as phononic metamaterials. The postbuckling analysis shows that the elastic wave bandgaps of the chiral hierarchical structures can be more effectively tuned in a wide range of frequency due to the chiral buckling mechanism. They possess a lower critical buckling strain than the corresponding symmetric hierarchical structures. Another prominent advantage of the chiral hierarchical structures lies in that they may keep a constant number of elastic wave bandgaps during the postbuckling process under a wide range of strain. Due to these features, chiral hierarchical structures hold promises for significant applications as phononic metamaterials.

In addition, it is expected that chiral hierarchical structure can also be used as, for examples, acoustic vortex metamaterials [47], pneumatic-driven [29,42], opto-driven [48] flexibly functional metamaterials. Topology optimization [49,50] and machine learning methods [51–53] would help to conduct function-oriented design for soft hierarchical structures. These interesting issues deserve further research.

Declaration of competing interest

The authors declare that they have no known competing financial interests or personal relationships that could have appeared to influence the work reported in this paper.

Acknowledgments

Supports from the National Natural Science Foundation of China (Grant Nos. 11921002 and 12032104) are acknowledged. The authors also wish to thank the great help of Dr. Bo Li, Sifan Yin, and Zhaoyi Zhang from Tsinghua University.

References

- [1] M.H. Lu, L. Feng, Y.F. Chen, Phononic crystals and acoustic metamaterials, *Mater. Today* 12 (12) (2009) 34–42.
- [2] J.Y. Liu, H.B. Guo, T. Wang, A review of acoustic metamaterials and phononic crystals, *Crystals* 10 (4) (2020) 305.
- [3] A. Clausen, F.W. Wang, J.S. Jensen, O. Sigmund, J.A. Lewis, Topology optimized architectures with programmable Poisson's ratio over large deformations, *Adv. Mater.* 27 (2015) 5523–5527.
- [4] C. Coulais, J.T.B. Overvelde, L.A. Lubbers, K. Bertoldi, M. van Hecke, Discontinuous buckling of wide beams and metabeams, *Phys. Rev. Lett.* 115 (2015) 044301.
- [5] L.S. Jin, A.E. Forte, B.L. Deng, A. Rafsanjani, K. Bertoldi, Kirigami-inspired inflatables with programmable shapes, *Adv. Mater.* 32 (2020) 2001863.
- [6] B. Li, Y.P. Cao, X.Q. Feng, H.J. Gao, Mechanics of morphological instabilities and surface wrinkling in soft materials: a review, *Soft Matter* 8 (2012) 5728–5745.
- [7] D. Yang, et al., Buckling pneumatic linear actuators inspired by muscle, *Adv. Mater. Technol.* 1 (2016) 1600055.
- [8] B. Gorissen, D. Melancon, N. Varios, M. Torbati, K. Bertoldi, Inflatable soft jumper inspired by shell snapping, *Sci. Robotics* 5 (42) (2020) eabb1967.
- [9] J. Vaicekauskaitė, C.H. Yang, A.L. Skov, Z.G. Suo, Electric field concentration in hydrogel-elastomer devices, *Extrem. Mech. Lett.* 34 (2020) 100597.
- [10] K. Liu, S.T. Chen, F.F. Chen, X.Y. Zhu, A unidirectional soft dielectric elastomer actuator enabled by built-in honeycomb metastructures, *Polymers* 12 (3) (2020) 619.
- [11] M. Li, H.X. Zhang, Z.L. Zhao, X.Q. Feng, Surface effects on cylindrical indentation of a soft layer on a rigid substrate, *Acta Mech. Sinica* 36 (2020) 422–429.
- [12] A.S. Gladman, E.A. Matsumoto, R.G. Nuzzo, L. Mahadevan, J.A. Lewis, Biomimetic 4D printing, *Nature Mater.* 15 (2016) 413–418.
- [13] X.F. Xue, et al., Mechanics-guided embryonic patterning of neuroectoderm tissue from human pluripotent stem cells, *Nature Mater.* 17 (2018) 633–641.
- [14] M.F. Zhu, et al., In vivo engineered extracellular matrix scaffolds with instructive niches for oriented tissue regeneration, *Nature Commun.* 10 (1) (2019) 1–14.
- [15] C. Mota, S. Camarero-Espinosa, M.B. Baker, P. Wiering, L. Moroni, Bioprinting: from tissue and organ development to in vitro models, *Chem. Rev.* 120 (2020) 10547–10607.
- [16] J.Y. Huang, X.D. Wang, Z.L. Wang, Controlled replication of butterfly wings for achieving tunable photonic properties, *Nano Lett.* 6 (2006) 2325–2331.
- [17] K.S. Liu, L. Jiang, Bio-inspired design of multiscale structures for function integration, *Nano Today* 6 (2011) 155–175.
- [18] B.D. Wilts, et al., Butterfly gyroid nanostructures as a time-frozen glimpse of intracellular membrane development, *Sci. Adv.* 3 (2017) e1603119.
- [19] J. Aizenberg, V.C. Sundar, A.D. Yablon, J.C. Weaver, G. Chen, Biological glass fibers: correlation between optical and structural properties, *Proc. Natl. Acad. Sci. USA* 101 (2004) 3358–3363.

- [20] M.C. Fernandes, J. Aizenberg, J.C. Weaver, K. Bertoldi, Mechanically robust lattices inspired by deep-sea glass sponges, *Nature Mater.* (2020) <http://dx.doi.org/10.1038/s41563-020-0798-1>.
- [21] G.L. Ying, et al., Bioprinted injectable hierarchically porous gelatin methacryloyl hydrogel constructs with shape-memory properties, *Adv. Funct. Mater.* 30 (46) (2020) 2003740.
- [22] G.L. Bluhm, O. Sigmund, F.W. Wang, K. Poulios, Nonlinear compressive stability of hyperelastic 2D lattices at finite volume fractions, *J. Mech. Phys. Solids* 137 (2020) 103851.
- [23] W.W. Wu, W.X. Hu, G.A. Qian, H.T. Liao, X.Y. Xu, F. Berto, Mechanical design and multifunctional applications of chiral mechanical metamaterials: a review, *Mater. Des.* 180 (2019) 107950.
- [24] T. Frenzel, M. Kadic, M. Wegener, Three-dimensional mechanical metamaterials with a twist, *Science* 358 (2017) 1072–1074.
- [25] H.K. Zhang, Y.J. Luo, Z. Kang, Bi-material microstructural design of chiral auxetic metamaterials using topology optimization, *Compos. Struct.* 195 (2018) 232–248.
- [26] H.Z. Li, et al., Spontaneous droplets gyrating via asymmetric self-splitting on heterogeneous surfaces, *Nature Commun.* 10 (2019) 1–6.
- [27] D.P. Richman, R.M. Stewart, J.W. Hutchinson, V.S. Caviness, Mechanical model of brain convolutional development, *Science* 189 (1975) 18–21.
- [28] A. Sapala, et al., Why plants make puzzle cells, and how their shape emerges, *Elife* 7 (2018) e32794.
- [29] D. Yang, et al., Buckling of elastomeric beams enables actuation of soft machines, *Adv. Mater.* 27 (41) (2015) 6323–6327.
- [30] H. Zhang, X. Cheng, D.J. Yan, Y.H. Zhang, D.N. Fang, A nonlinear mechanics model of soft network metamaterials with unusual swelling behavior and tunable phononic band gaps, *Compos. Sci. Technol.* 183 (2019) 107822.
- [31] X.J. Tan, et al., Real-time tunable negative stiffness mechanical metamaterial, *Extrem. Mech. Lett.* 41 (2020) 100990.
- [32] M.B. Jackson, W. Armstrong, Formation of aerenchyma and the processes of plant ventilation in relation to soil flooding and submergence, *Plant Biol.* 1 (3) (1999) 274–287.
- [33] J. Jung, S.C. Lee, H.K. Choi, Anatomical patterns of aerenchyma in aquatic and wetland plants, *J. Plant Biol.* 51 (2008) 428–439.
- [34] K. Bertoldi, M.C. Boyce, Mechanically triggered transformations of phononic band gaps in periodic elastomeric structures, *Phys. Rev. B* 77 (5) (2008) 052105.
- [35] P. Wang, J.M. Shim, K. Bertoldi, Effects of geometric and material nonlinearities on tunable band gaps and low-frequency directionality of phononic crystals, *Phys. Rev. B* 88 (2013) 014304.
- [36] Y. Zheng, G.Y. Li, Y.P. Cao, X.Q. Feng, Wrinkling of a stiff film resting on a fiber-filled soft substrate and its potential application as tunable metamaterials, *Extrem. Mech. Lett.* 11 (2017) 121–127.
- [37] Y.L. Huang, N. Gao, W.Q. Chen, R.H. Bao, Extension/compression-controlled complete band gaps in 2D chiral square-lattice-like structures, *Acta Mech. Solida Sin.* 31 (2018) 51–65.
- [38] C.H. Feng, Q. Li, Y.J. Zeng, X. Su, H.B. Yu, 2D to 3D convertible terahertz chiral metamaterial with integrated pneumatic actuator, *Opt. Express* 26 (2018) 14421–14432.
- [39] Y.X. Chen, B. Ai, Z.J. Wong, Soft optical metamaterials, *Nano Convergence* 7 (2020) 1–17.
- [40] H.K. Zhang, W.J. Wu, Z. Kang, X.Q. Feng, Topology optimization method for the design of bioinspired self-similar hierarchical microstructures, *Comput. Methods Appl. Mech. Engrg.* 372 (2020) 113399.
- [41] B. Li, Y.P. Cao, X.Q. Feng, H.J. Gao, Surface wrinkling of mucosa induced by volumetric growth: theory, simulation and experiment, *J. Mech. Phys. Solids* 59 (2011) 758–774.
- [42] D. Guo, Z. Kang, Chamber layout design optimization of soft pneumatic robots, *Smart Mater. Struct.* 29 (2020) 025017.
- [43] L.R. Meza, A.J. Zelhofer, N. Clarke, A.J. Mateos, D.M. Kochmann, J.R. Greer, Resilient 3D hierarchical architected metamaterials, *Proc. Natl. Acad. Sci. USA* 112 (2015) 11502–11507.
- [44] M.G. Tarantino, K. Danas, Programmable higher-order Euler buckling modes in hierarchical beams, *Int. J. Solids Struct.* 167 (2019) 170–183.
- [45] Z. Vangelatos, G.X. Gu, C.P. Grigoropoulos, Architected metamaterials with tailored 3D buckling mechanisms at the microscale, *Extrem. Mech. Lett.* 33 (2019) 100580.
- [46] J.Y. Zeng, et al., Moth wing scales slightly increase the absorbance of bat echolocation calls, *PLoS One* 6 (11) (2011) e27190.
- [47] H. Zhang, Y. Gao, Acoustic vortex beam generation by a piezoelectric transducer using spiral electrodes, *Chin. Phys. Lett.* 36 (11) (2019) 114302.
- [48] Z.M. Hu, W. Fang, Q.Y. Li, X.Q. Feng, J.A. Lv, Optocapillarity-driven assembly and reconfiguration of liquid crystal polymer actuators, *Nature Commun.* 11 (2020) 5780.
- [49] N. Aage, E. Andreassen, B.S. Lazarov, O. Sigmund, Giga-voxel computational morphogenesis for structural design, *Nature* 550 (2017) 84–86.
- [50] H.K. Zhang, Z. Kang, Y.Q. Wang, W.J. Wu, Isotropic quasi-fluid metamaterials designed by topology optimization, *Adv. Theory Simul.* 3 (2020) 1900182.
- [51] S. Ye, B. Li, Q.Y. Li, H.P. Zhao, X.Q. Feng, Deep neural network method for predicting the mechanical properties of composites, *Appl. Phys. Lett.* 115 (2019) 161901.
- [52] X.H. Jiang, F. Liu, X.T. Wang, L.F. Wang, Machine learning-based design and optimization of curved beams for multistable structures and metamaterials, *Extrem. Mech. Lett.* 41 (2020) 101002.
- [53] L.W. Wang, Y.C. Chan, F. Ahmed, Z. Liu, P. Zhu, W. Chen, Deep generative modeling for mechanistic-based learning and design of metamaterial systems, *Comput. Methods Appl. Mech. Engrg.* 372 (2020) 113377.